Observations of x-ray spectra from highly charged tungsten ions in tokamak plasmas

R. Neu, K.B. Fournier, D. Schlögl, J. Rice

IPP 10/7 June 1997

MAX-PLANCK-INSTITUT FÜR PLASMAPHYSIK

85748 GARCHING BEI MÜNCHEN

MAX-PLANCK-INSTITUT FÜR PLASMAPHYSIK

GARCHING BEI MÜNCHEN

Observations of x-ray spectra from highly charged tungsten ions in tokamak plasmas

R. Neu, K.B. Fournier, D. Schlögl, J. Rice

IPP 10/7 June 1997

Die nachstehende Arbeit wurde im Rahmen des Vertrages zwischen dem Max-Planck-Institut für Plasmaphysik und der Europäischen Atomgemeinschaft über die Zusammenarbeit auf dem Gebiete der Plasmaphysik durchgeführt.

Observations of x-ray spectra from highly charged tungsten ions in tokamak plasmas

R.Neu, K.B. Fournier*, D. Schlögl, J. Rice†

Max-Planck-Institut für Plasmaphysik, IPP-EURATOM Association
85748 Garching, Germany

Abstract

X-ray spectra in the range from 7 to 10 Å from highly charged tungsten (Z=74) ions were observed in the tokamak ASDEX Upgrade. Lines emitted from W^{37+} to W^{47+} were identified by comparison with *ab initio* calculations and with the expected ionisation equilibrium charge state distribution. Most of the features in the observed spectra coincide with predicted lines. A spectral line of AsI-like W^{41+} could be identified as the predominant one for plasmas with 2.5 to 3 keV central electron temperature. The calculations predict clearly separated spectral lines for KrI-like W at about 18.4 Å and strong lines between 5.6 and 6.0 Å for all charge states under consideration that can be used for monitoring W densities in the soft x-ray region. Tungsten concentrations in the range of 10^{-4} were extracted from the emissivities of spectral lines from W^{40+} and W^{41+}.

*Lawrence Livermore National Laboratory, Livermore, California 94550, USA

†Plasma Science and Fusion Center, Massachusetts Institute of Technology, Cambridge, Massachusetts 02139-4307, USA

1 Introduction

There is a renewed interest in the use of high-Z plasma facing components in the next generation of magnetically confined fusion devices [1]. Due to its high radiation power, it has been claimed that its fractional abundance in the plasma of a fusion device should be kept below 10^{-4} [2]. More recent estimates for the allowed central impurity radiation in the planned International Thermo-Nuclear Experimental Reactor (ITER) [3] point to a value lower by almost a factor of 10. The radiation loss parameter from an average ion model [4, 5] is used in calculations for the allowed concentrations in future devices, as well as directly [6, 7] or indirectly [8, 9] in the calculation of W concentrations in plasmas of present day tokamaks. W-concentrations in the range of 10^{-4} normally do not cause severe problem in these machines since, in contrast to ITER, there are no requirements due to an optimized fusion product or the central electron density and moreover the volumetric heating power is often larger. However, one ought to be careful using the radiation loss parameter, because detailed investigations of the radiation from and the ionisation equilibria of Mo ions in the tokamaks Alcator C-Mod [10] and FTU [11] reveal strong deviations from the conventional coronal equilibrium predictions [12] due to the effect of excitation-autoionisation (EA) and therewith also changes in the radiation power across the plasma.

Previous investigations of tungsten radiation in tokamaks have dealt with lower charge states than those reported here [13, 14]. These give rise to the 4d - 4f quasi-continuum radiation (N-shell Δn=0 transitions) which has long been known to dominate the tungsten impurity emission spectra [15] and to be correlated with hollow temperature profiles [16] and disruption of plasma current profiles. The present work reports on observations in hotter plasmas than those studied in Refs [13, 14], and in a higher energy spectral region. Observations and calculations of $3l$ - $4l'$ lines (M-shell Δn=1 transitions) and calculations of $4l$ - $5l'$ lines (N-shell Δn=1 transitions) are presented here. Magnetically confined fusion plasma experiments are achieving higher temperatures and longer energy confinement times. Thus, there is a strong need for an experimental investigation of the radiation losses from higher tungsten charge states, as well as for spectroscopic information for diagnostic purposes that is independent of (sometimes uncertain) radiation power models (see sec. IV, below).

There are several publications on observations of soft x-ray spectral lines of highly charged ions of W from laser produced plasmas in the range from 3.4 to 4.5 Å [17, 18], from 6.7 to 7.3 Å [19, 20] and above 10 Å [21]. Recently, high resolution measurements of spectral lines from NiI-like W at 7.17 Å were reported from an electron beam ion trap (EBIT) experiment [22].

The present paper will present measurements from a tokamak (ASDEX Upgrade) plasma in the spectral range from 7 to 10 Å, together with *ab initio* calculations. From

the comparison of the theoretical and the measured emissivities of two spectral lines the W-density will be calculated.

2 Experiment Description

ASDEX Upgrade [23] is a mid sized tokamak R=1.65 m, a=0.5 m with an elongated plasma ($\kappa = 1.6$) and a magnetic divertor. In addition to ohmic heating, up to 10 MW through neutral beam injection and up to 4 MW via ion cyclotron radio frequency heating are available. Central electron temperatures near 3 keV and line averaged electron densities around $10^{20}/m^3$ were typically achieved during the tungsten injection experiments.

The tungsten is injected into the plasma discharges via a laser ablation system [24] that produces a quasicontinuous influx of tungsten. A target made of a 0.3 μm - 1.0 μm W-film evaporated on a thin glass plate is irradiated with the beam of a 20 Hz, 0.6 J/pulse Nd-YAG laser from the back side. The injected amount of tungsten is estimated from the ablation spot to be about 0.5×10^{17} particles/pulse. The laser beam is deflected on the target to allow about 30 injections during one plasma discharge. Since the impurity transport time in most discharges is larger than 50 ms [24], the injections result in an almost constant W inventory in the plasma discharge over 1-2 seconds. This is of great importance since the spectral lines are measured with a rotating crystal Bragg spectrometer [25] with a slow recording time. The flat crystal is mounted on a revolver allowing the use of 6 different crystals that can be changed in between two plasma discharges. The crystals used for this work were KAP ($2d = 26.58$Å) and ADP ($2d = 10.64$ Å). The x-rays are detected with a proportional counter of the microstrip gaseous chamber (MSGC) type [26] which allows count rates above 1 MHz and subsequent pulse height discrimination. The crystal as well as the detector are rotated during the plasma discharge. Depending on the chosen rotation frequency and the rotation angles, a complete spectrum takes about 3 seconds to record. This means that the different wavelengths are measured sequentially and therefore almost constant plasma parameters must be maintained during the measurement. The advantage of the system is that a whole spectrum from about 7 Å to about 20 Å, in the case of the KAP crystal, could be recorded during one single plasma discharge. The crystal angle and the detector angle are monitored continuously. The wavelength calibration of the system is performed using spectral lines of intrinsic impurities. Errors in the wavelengths are due to the jitter in the rotation which is found to be about 0.03°. This gives an error of about 0.015 Å at a wavelength of 7 Å using the KAP crystal.

The temporal behavior of the plasma parameters of one of the discharges used for the W measurements is shown in Fig. 1. The traces on the top show the spectrum measured during the rotation of the ADP crystal and the monitored crystal angle (Θ_C)

that translates to the wavelength. The second row shows a line integral of the total radiation (P_{rad}), where every tungsten injection could be identified as a spike. The central soft x-ray radiation (P_{SXR}, $E_{rad} \geq 1$ keV, third row) exhibits strong variations due to sawtooth instabilities. These have also an impact on the W - line intensities because of the rapid decrease of the central electron temperature. The time averaged central temperature (T_{e0}, fourth row), the line averaged central density ($\bar{n}_e$, fifth row), as well as the plasma current ($I_P = 0.8$ MA, not shown in the figure) stayed (almost) constant throughout the tungsten measurement. The lowest trace in the figure represents the auxiliary heating power (5 MW) injected by neutral beams (P_{NBI}).

3 Tungsten Calculations

The majority of line emission in the 7 to 10 Å region is composed of $3l \rightarrow 4l'$ transitions. Identification of the line features is achieved by comparison of the observed spectra with *ab initio* atomic structure calculations and predictions of the collisional-radiative line emissivities. The atomic structure calculations are done with the fully relativistic parametric potential code RELAC of Klapisch [27, 28, 29]. For a given ion, RELAC determines an analytic form for the ionic potential by minimizing the average energy of a configuration of a group of configurations. Once the wavefunctions which minimize the configuration-average energy have been found, RELAC calculates the multi-configuration, intermediate coupled energy eigenvalues, including Briet interaction energy, vacuum polarization and Lamb shift corrections, of the fine structure levels as well as the transition rates and oscillator strengths for any multipole operator [30] requested. In the present work, each calculation included the ground configuration ($3s^2 3p^6 3d^9$ for CoI-like W^{47+} to $4s^2 4p^6 4d^1$ for RbI-like W^{37+}) and excitations from the 3p and 3d orbitals to all available $4l'$ and $5l'$ ($l' = 0,1,2,3$) orbitals. (In the case of W^{47+}, 3s to $4l'$ excitations were also considered.) RELAC's wavefunctions are then used by the quasi-relativistic code CROSS [31] to compute collisional excitation rates between all the levels of a given ion in the distorted wave approximation. CROSS is able to accomplish this using the factorization theorem of Bar-Shalom, Klapisch and Oreg in conjunction with a semi-empirical interpolation scheme [31]. The collision rates and the electric and magnetic dipole and quadrupole transition (E1, M1, E2 and M2, respectively) rates are then used to find the steady state collisional-radiative level populations in each ion.

In the case of E1 emission features, there is a correlation between oscillator strength and the predicted emissivity [10, 32]; in this case, the lines with the strongest E1 oscillator strengths will have the brightest emissivities, and the RELAC calculations alone are adequate to the job at hand. Other multipole transitions (M1, E2 and M2) have small oscillator strengths, but originate from highly populated (metastable) levels and can be

quite bright. In this case, the full collisional-radiative prediction of transition emissivity is required to classify spectral features. For example, the NiI-like W^{46+} line (observed) at 7.93 Å is a ΔJ=2 3d $\rightarrow$ 4s E2 decay, and is seen to be very bright. For the correct population distribution amongst the levels of the ground configurations in each ion, M1, E2 and M2 decays are essential, and, in the related VUV spectra of each ion [9], lines which arise from M1 decays may be visible. Figure 2a shows the calculated transitions in the wavelength range from 4 to 10 Å, from the tungsten charge states between KrI-like W^{38+} and CoI-like W^{47+}. The line intensities are calculated from the collisional-radiative model at the temperatures indicated in the figure. Each individual line is given a 1/e width of 0.02 Å. The strongest lines are located near 6 Å, and decrease monotonically in wavelength as the charge state increases. Shown in Figure 2b are the calculated spectra between 10 and 20 Å. In contrast to the lower wavelength range here there are only a few lines emitted from the charge states under consideration. The $4p_{3/2} \rightarrow 5s_{1/2}$ line from KrI-like W^{38+} at 18.4 Å is nicely isolated and by far the strongest. The complete tabulation of x-ray (and VUV) transitions in tungsten charge states between W^{37+} and W^{47+} is presented in Ref. [33].

4 Measured Tungsten X-ray Spectra

The calculated x-ray line emissivities for each ion have been compared to the observed emission features. Figure 3a shows a measured spectrum from 7.0 to 8.5 Å, with the background subtracted, obtained with the KAP crystal during a 1 MA, 2.5 T discharge with a central electron temperature of $T_{e0} \approx 2.7$ keV and line averaged electron density $\bar{n}_e = 1.1 \times 10^{20}/\mathrm{m}^3$ with 7.5 MW additional heating through NBI. In this discharge, there was only one tungsten injection at the start of the recording of the spectrum and the W density decayed slowly during the time period in which this spectrum was obtained. The spectra are recorded twice in two subsequent discharges with and without W injection to look for the contribution of spectral lines from intrinsic impurities. The remaining large background in the first part of the spectrum is due to contributions from zeroth order reflection of UV light decaying quickly after the injection. There is a large conglomeration of W lines between 7.0 and 7.7 Å, and an isolated line at 7.93 Å (E2) from the closed-shell NiI-like W^{46+}. Measured wavelengths of the individual features of this spectrum, along with line identifications and theoretical wavelengths are presented in Table I. The wavelengths of all major transitions are in excellent agreement taking into account the experimental error of about 0.015Å. Shown at the bottom of Fig. 3a are calculated spectra of tungsten charge states between BrI-like W^{39+} and NiI-like W^{46+}, and most of the features in the observed spectrum coincide with predicted lines. Figure 3b shows a measured spectrum from 7.0 to 7.8 Å, with the background subtracted, obtained with

the ADP crystal during a 0.8 MA, 2 T discharge with a central electron temperature of $T_{e0} \approx 3$ keV, a line averaged electron density $\bar{n}_e = 0.6 \times 10^{20}/\mathrm{m}^3$ and with 5 MW additional heating through NBI. In this case the W density was kept almost constant through multiple injections. The background through reflected UV lines was much less due to the larger Bragg angle of the ADP crystal at this wavelength and a higher discriminator level. Again, individual lines from tungsten charge states between CuI-like and BrI-like are clearly identifiable. This discharge however, showed strong sawtooth instabilities during the recording of the spectrum (see Fig. 1). Due to the rapid decrease of the central temperature during the sawtooth crash, a suppression of the line radiation at 7.5 Å and 7.9 Å was found.

Besides the line at 9.18 Å from W^{45+}, which could be observed with both crystals, no strong lines are found in the range from 8.5 to 10 Å (see Fig. 1). This is also in good agreement with the theoretical predictions. The predominant transition in Fig. 3 arises from AsI-like W^{41+}. For central electron temperatures around 3 keV, from the predictions of coronal equilibrium, one would expect to see charge states up to CoI-like W^{47+} [12]. Additionally, in similar discharges, VUV transitions in the range from 45 to 65 Å and 120 to 140 Å could be identified as arising from Br- to GaI-like ionisation states [9] which agrees well with the shown spectra.

Caution must be used when making a quantitative comparison with the line intensities. As mentioned above the different portions of these spectra were obtained at different times during the discharges, which were evolving either through decaying of the overall tungsten density (discharge #6540 shown in Fig. 3a) or through strong sawtooth activity (discharge #8410 shown in Fig. 3b and Fig. 1). Therefore it was not attempted to simulate the total intensities of the whole spectra, but only the line intensities calculated as described in paragraph III were shown in Fig. 3, disregarding the individual fractional abundance of the charge states as well as the actual temperature profile.

Nevertheless a first attempt was carried out to extract the W density from the emissivity of spectral lines at 7.41 Å from the AsI-like tungsten and at 7.48 Å from the SeI-like ionisation states for discharge #6540. (The spectral line at 7.94 Å from NiI-like tungsten arises from a E2 transition and is not fed primarily from excitations from the ground level.) The absolute calibration [25] for the Bragg spectrometer, which is uncertain within a factor of 2, yields measured emissivities of 2.9 $\mathrm{W}/(\mathrm{m}^2\mathrm{sr})$ and 1.3 $\mathrm{W}/(\mathrm{m}^2\mathrm{sr})$, respectively. Using radial profiles for n_e and T_e, the line of sight integrated value of the brightness could be calculated as

$$I_{calc} = \frac{1}{4\pi} \int_\ell n_W f_{Wxx} n_e X_W ds \ , \qquad (1)$$

with the profiles of the corresponding fractional abundance f_{Wxx} of ion W^{xx} found from transport calculations and where the excitation rate coefficient X_W is calculated

[31] on a fine temperature grid. A comparison of the calculated and measured values for the emissivity yields total W densities n_W of $1.7 \cdot 10^{16}/\mathrm{m}^3$ and $1.4 \cdot 10^{16}/\mathrm{m}^3$, respectively. These values correspond to total W concentrations of $1.8 \cdot 10^{-4}$ and $1.6 \cdot 10^{-4}$ at the radial position of $r/a \approx 0.3 - 0.4$ where the maximum of the volumetric emissivity of W^{40+} and W^{41+} is found. The W-concentrations could also be calculated from the total measured radiation using the radiation loss parameter [4, 5]. In this discharge at $r/a \approx 0.3 - 0.4$ a local W-concentration is deduced, which is smaller by a factor of 4 compared to the concentration from the W^{41+} lines. However the radiation profile has a strongly localized maximum at the plasma center leading to central concentrations of about $2 \cdot 10^{-4}$, which is in good agreement with the above values. Since the radiation profile results from an elaborate deconvolution, the discrepancy at $r/a \approx 0.3 - 0.4$ could be due to problems of the unfolding procedure as well as from the spectrometer calibration or the atomic physics parameters.

5 Conclusions

Tungsten x-ray spectra between 7 and 10 Å were obtained from the ASDEX Upgrade tokamak with a rotating crystal spectrometer system. These were compared with *ab initio* calculations of charge states between W^{38+} and W^{46+}. Individual lines of all ionisation states were identified, and a transition of Arsenic-like W^{41+} is predominant in this wavelength range for the 3 keV plasmas under consideration. The measurements and the calculations show an excellent agreement for the wavelengths which gives confidence in the theoretical predictions. They suggest that for plasma temperatures below 2 keV the spectral line of KrI-like W at ≈ 18.4 Å would be best suited for monitoring W in the x-ray region. For temperatures above 3 keV the transitions at ≈ 5.6 Å in CoI-like or NiI-like W might be preferable. Spectral lines from AsI-like and SeI-like W were used to deduce W densities. There is an excellent agreement between the W-concentrations extracted from the different spectral lines, but the values differ by about a factor of 4 from the local W densities calculated from the radiation loss parameter. Although the reason for this difference is not yet resolved, it is obvious that the extraction of the W concentration using spectral lines can be superior to the method using the total radiation, because of the more direct evaluation of the experimental data and the more specific atomic physics which can be applied. To investigate the consistency of the measurements, other diagnostic spectral lines, which are emitted from different temperature ranges, will be searched in future experiments.

6 Acknowledgements

The authors like to thank K. Asmussen for fruitful discussions, R. Dux for assisting the W transport calculations and J.C. Fuchs for supplying the profiles of the total radiation. We are also grateful to the ASDEX Upgrade team for expert running of the tokamak. Work supported at MIT by DoE Contract No. DE-AC02-78ET51013 and at LLNL by DoE Contract No. W-7405-ENG-48.

References

[1] N. Noda, V. Philipps, and R. Neu, to be published J. Nucl. Mater. (1996).

[2] R. Jensen, D. Post, and D. Jassby, Nucl. Sci. Eng. **65**, 282 (1978).

[3] N. Peacock *et al.*, in *Diagnostics for experimental thermonuclear fusion reactors, Varenna (Italy)*, edited by P. Stott, G. Giuseppe, and E. Sindoni (Plenum Press, New York, 1996), pp. 291 — 305.

[4] D. Post *et al.*, At. Data Nucl. Data Tables **20**, 397 (1977).

[5] D. Post, J. Abdallah, R. Clark, and N. Putvinskaya, Phys. Plasmas **2**, 2328 (1995).

[6] V. Philipps *et al.*, *Europhysics Conference Abstracts (Proc. of the 22th EPS Conference on Controlled Fusion and Plasma Physics, Bournemouth, 1995)* (EPS, Geneva, 1995), Vol. 19C, part II, pp. 321–324.

[7] J. Rapp *et al.*, *Europhysics Conference Abstracts (Proc. of the 23th EPS Conference on Controlled Fusion and Plasma Physics, Kiev, 1996)* (EPS, Geneva, YEAR), Vol. 20C, pp. 819 — 822.

[8] K. Asmussen, Technical Report No. 10/2, IPP, Garching, Germany, (unpublished), ph.D. thesis TU Munich, June 95.

[9] K. Asmussen *et al.*, to be published .

[10] J. Rice *et al.*, J. Phys. B. **29**, 2191 (1996), and references therein.

[11] K. Fournier *et al.*, , to appear in Nucl. Fusion **37**, No. 6 (1997).

[12] C. Breton, C. DeMichelis, M. Finkenthal, and M. Mattioli, Technical Report No. 948, EURATOM-CEA-FC (unpublished).

[13] M. Finkenthal *et al.*, Phys. Lett. A **127**, 255 (1988).

[14] P. Mandelbaum, J. Schwob, M. Finkenthal, and M. Klapisch, Journal de Physique **49**, cl ((1988)).

[15] E. Hinnov *et al.*, Nucl. Fusion **18**, 1305 (1978).

[16] V. Arunasalam *et al.*, *Proc. 8th Conf. EPS, Prague 1977* (EPS, Geneva, 1978), Vol. 2, pp. 17–28.

[17] A. Zigler, M. Klapisch, and P. Mandelbaum, Phys. Lett. A **117**, 31 (1986).

[18] N. Tragin *et al.*, Phys. Scr. **37**, 72 (1987).

[19] A. Zigler *et al.*, J. Opt. Soc. Am. **70**, 129 (1980).

[20] P. Mandelbaum *et al.*, Phys. Scr. **27**, 39 (1983).

[21] J. Seely, C. Brown, and W. Behring, J. Opt. Soc. Am. **B6**, 3 (1989).

[22] S. Elliot, P. Beiersdorfer, B. MacGowan, and Nelson, Phys. Rev. A **52**, 2689 (1995).

[23] W. Köppendörfer *et al.*, in *Fusion Technology (Proc. of the 16th Symposium on Fusion Technology, London, U.K., 1990)*, edited by B. Keen, M. Huguet, and R. Hemsworth (Elsevier, Amsterdam, 1991), Vol. I, pp. 208–212.

[24] R. Neu *et al.*, in *Europhysics Conference Abstracts (Proc. of the 22th EPS Conference on Controlled Fusion and Plasma Physics, Bournemouth, 1995)*, edited by B. Keen, P. Stott, and J. Winter (EPS, Geneva, 1995), Vol. 19C, part I, pp. 65–68.

[25] D. Schlögl *et al.*, to be published .

[26] R. Neu *et al.*, Rev. Sci. Instrum. **67**, 1829 (1996).

[27] M. Klapisch, Computer Phys. Comm. **2**, 239 (1971).

[28] M. Klapisch, J. Schwob, B. Fraenkel, and J. Oreg, J. Opt. Soc. Am. **67**, 148 (1977).

[29] A. Bar-Shalom and M. Klapisch, Computer Phys. Comm. **50**, 375 (1988).

[30] I. Grant, J. Phys. B. **7**, 1458 (1974).

[31] A. Bar-Shalom, M. Klapisch, and J. Oreg, Phys. Rev. A **38**, 1773 (1988).

[32] R. Mewe, Astron. and Astrophys. **20**, 215 (1972).

[33] K. Fournier, , to appear in At. Data Nucl. Data Tables (summer, 1997).

e 1: Experimental and theoretical wavelengths of the identified transitions in tungsten

Ion	transition	$\lambda_{th.}$ (Å)	$\lambda_{exp.}$ (Å)
like W^{45+}	$(3d)^{10}(4s+)^1$ $J=1/2$ - $(3d)^9_{3/2}(4s+)^1(4p-)^1$ $J=1/2$	7.26	7.26
	and $(3d)^{10}(4s+)^1$ $J=1/2$ - $(3d)^9_{3/2}(4s+)^1(4p-)^1$ $J=3/2$	7.26	
like W^{43+}	$(3d)^{10}(4s)^2(4p-)^1$ $J=1/2$ - $(3d)^9_{5/2}(4s)^2(4p-)^1(4p+)^1$ $J=1/2$	7.28	7.26
	and $(3d)^{10}(4s)^2(4p-)^1$ $J=1/2$ - $(3d)^9_{5/2}(4s)^2(4p-)^1(4p+)^1$ $J=3/2$	7.28	
like W^{44+}	$(3d)^{10}(4s)^2$ $J=0$ - $(3d)^9_{3/2}(4s)^2(4p-)^1$ $J=1$	7.35	7.34
like W^{42+}	$(3d)^{10}(4s)^2(4p-)^2$ $J=0$ - $(3d)^9_{5/2}(4s)^2(4p-)^2(4p+)^1$ $J=1$	7.35	7.34
ike W^{41+}	$(3d)^{10}(4s)^2(4p-)^2(4p+)^1$ $J=3/2$ - $(3d)^9_{5/2}(4s)^2(4p-)^2(4p+)^2$ $J=3/2$	7.41	7.41
	and $(3d)^{10}(4s)^2(4p-)^2(4p+)^1$ $J=3/2$ - $(3d)^9_{5/2}(4s)^2(4p-)^2(4p+)^2$ $J=5/2$	7.42	
ike W^{40+}	$(3d)^{10}(4s)^2(4p-)^2(4p+)^2$ $J=2$ - $(3d)^9_{5/2}(4s)^2(4p)^5_{3/2}$ $J=3$	7.48	7.49
	and $(3d)^{10}(4s)^2(4p-)^2(4p+)^2$ $J=2$ - $(3d)^9_{5/2}(4s)^2(4p)^5_{3/2}$ $J=2$	7.48	
ike W^{39+}	$(3d)^{10}(4s)^2(4p)^5_{3/2}$ $J=3/2$ - $(3d)^9_{5/2}(4s)^2(4p-)^2(4p+)^4$ $J=5/2$	7.56	7.56
ike W^{39+}	$(3d)^{10}(4s)^2(4p-)^1(4p+)^3(4d-)^1$ $J=5/2$ - $(3d)^9_{3/2}(4s)^2(4p)^5_{3/2}(4d-)^1$ $J=3/2$	7.61	7.61
	$(3d)^{10}(4s)^2(4p-)^1(4p+)^3(4d-)^1$ $J=3/2$ - $(3d)^9_{3/2}(4s)^2(4p)^5_{3/2}(4d-)^1$ $J=3/2$	7.61	
	$(3d)^{10}(4s)^2(4p-)^1(4p+)^3(4d-)^1$ $J=1/2$ - $(3d)^9_{3/2}(4s)^2(4p)^5_{3/2}(4d-)^1$ $J=3/2$	7.61	
ike W^{39+}	$(3d)^{10}(4s)^2(4p-)^1(4p+)^3(4d+)^1$ $J=1/2$ - $(3d)^9_{5/2}(4s)^2(4p)^5_{1/2}(4d+)^1$ $J=3/2$	7.69	7.70
ike W^{46+}	$(3d)^{10}$ $J=0$ - $(3d)^9_{5/2}(4s+)^1$ $J=2$	7.94	7.93
ike W^{44+}	$(3d)^{10}(4s+)^1(4p-)^1$ $J=1$ - $(3d)^9_{5/2}(4s)^2(4p-)^1$ $J=3$	8.12	8.15
	and $(3d)^{10}(4s+)^1(4p-)^1$ $J=1$ - $(3d)^9_{5/2}(4s)^2(4p-)^1$ $J=2$	8.13	
ike W^{43+}	$(3d)^{10}(4s+)^1(4p-)^2$ $J=1/2$ - $(3d)^9_{5/2}(4s)^2(4p-)^2$ $J=5/2$	8.23	8.23
$W^{?+}$	?		8.33
ike W^{45+}	$(3d)^{10}(4p+)^1$ $J=3/2$ - $(3d)^9_{5/2}(4s)^2$ $J=5/2$	9.19	9.18

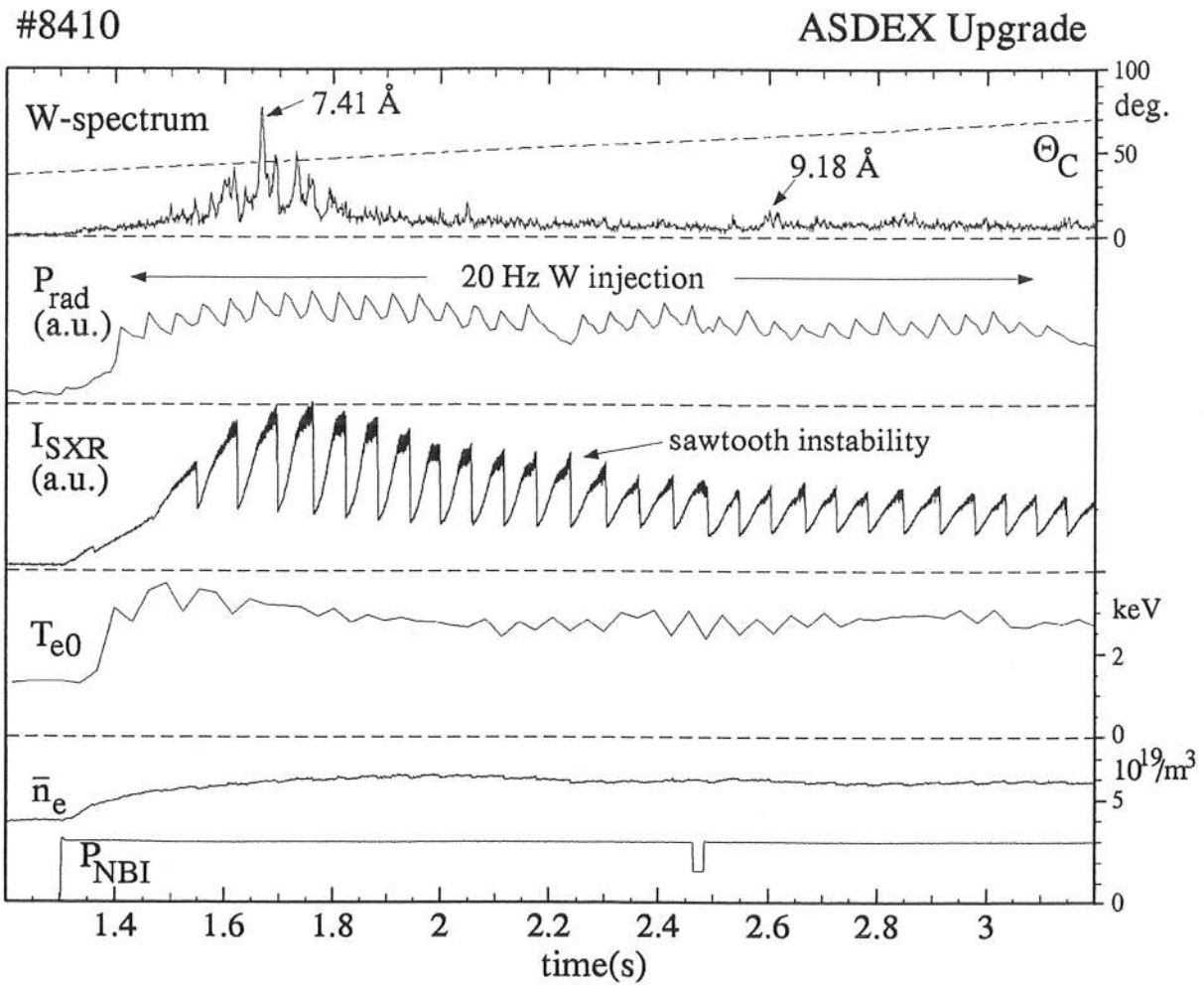

Figure 1: Temporal behavior of the line averaged electron density $\bar{n}_e$, power of the injected neutral beam P_{NBI}, central electron temperature T_{e0}, central soft x-ray intensity I_{SXR} and a line of sight integrated bolometric measurement of the total plasma radiation P_{Bolo} together with the recorded X-ray spectrum and the corresponding crystal angle Θ_C for the discharge #8410 with 20Hz W-injection.

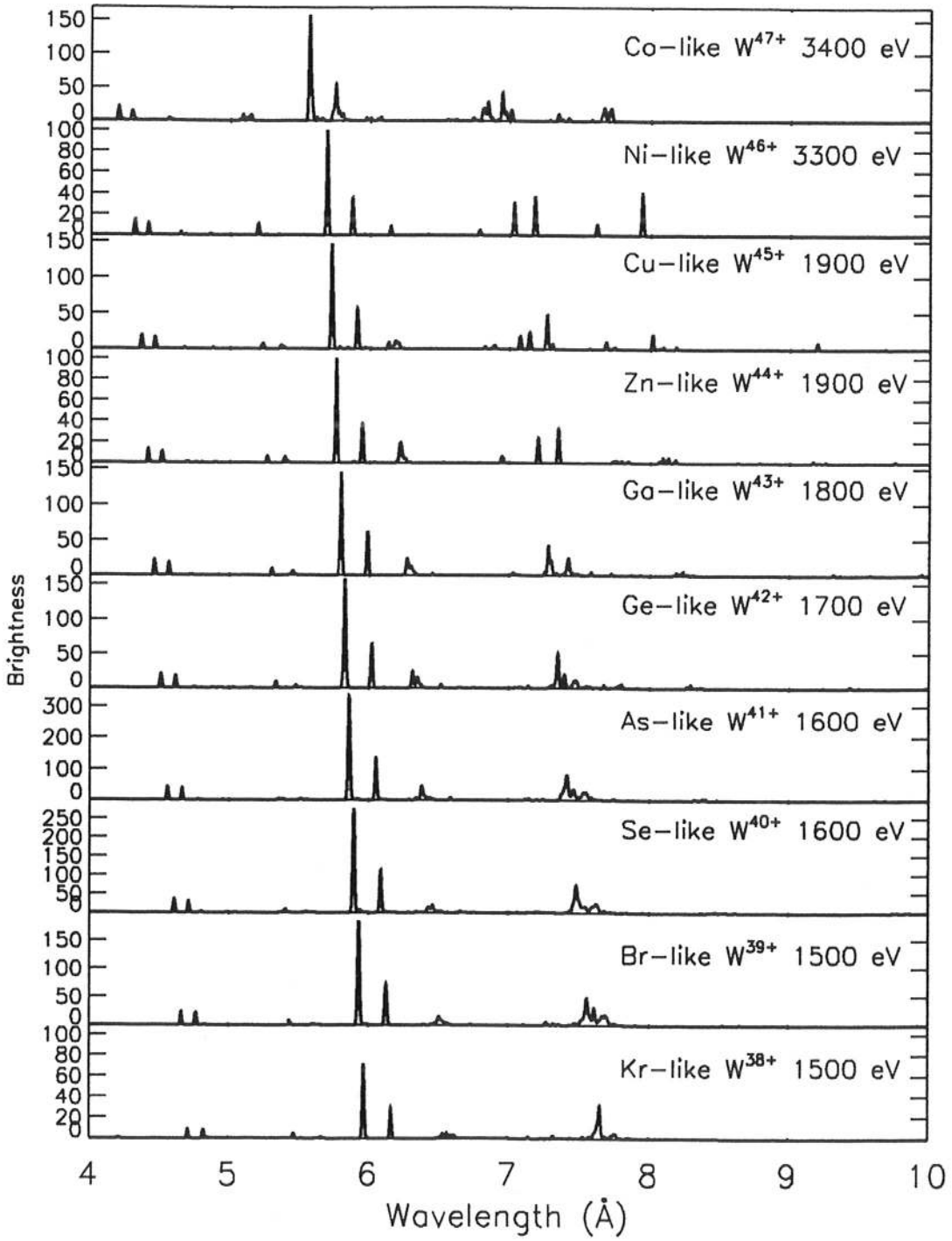

Figure 2: a) Calculated x-ray transitions for Kr - like to Co - like tungsten in the range of 4 Å to 10 Å.The line intensities are calculated from a collisional-radiative model at the temperatures indicated.

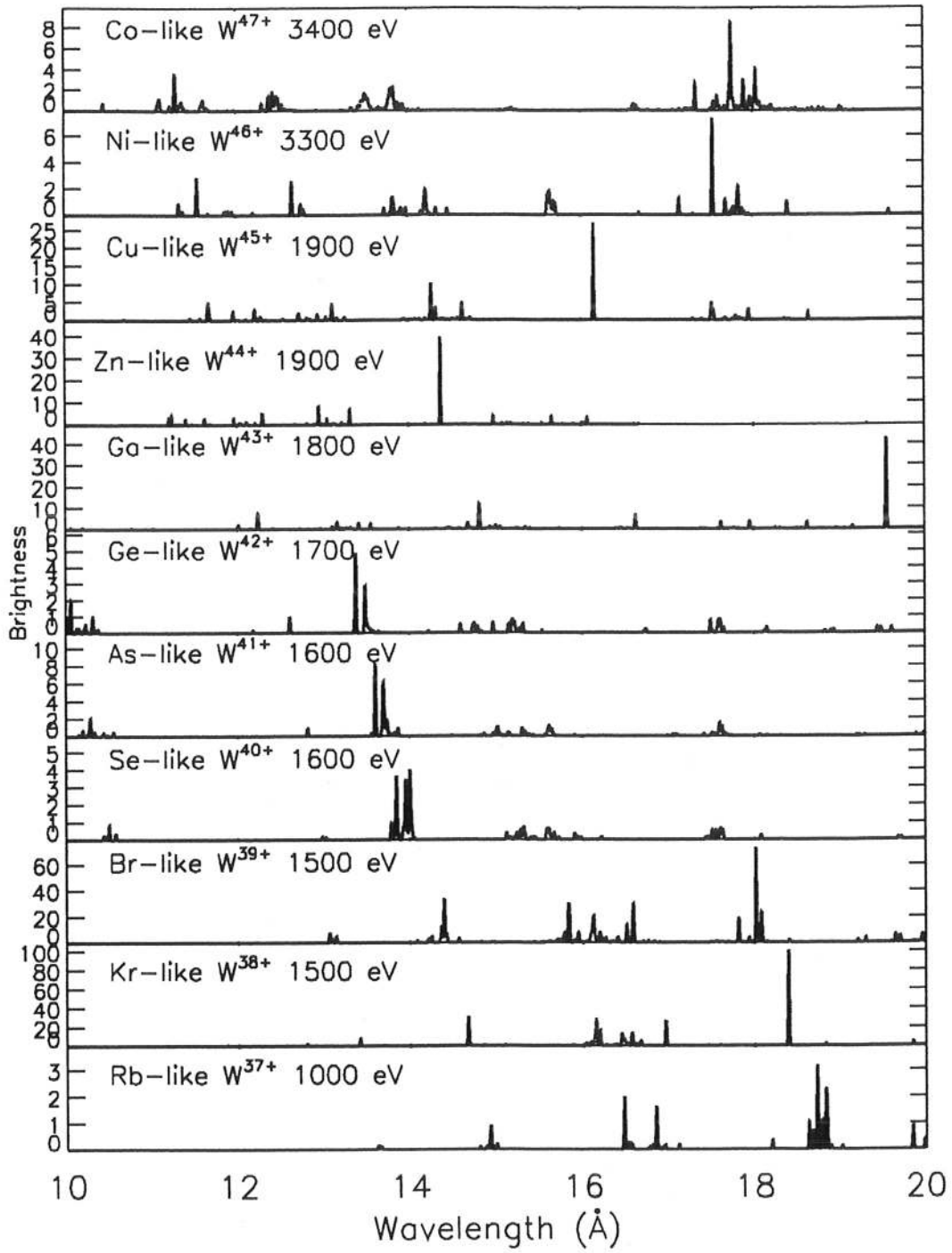

Figure 2: b) Calculated x-ray transitions for Rb - like to Co - like tungsten in the range of 10 Å to 20 Å. The line intensities are calculated from a collisional-radiative model at the temperatures indicated.

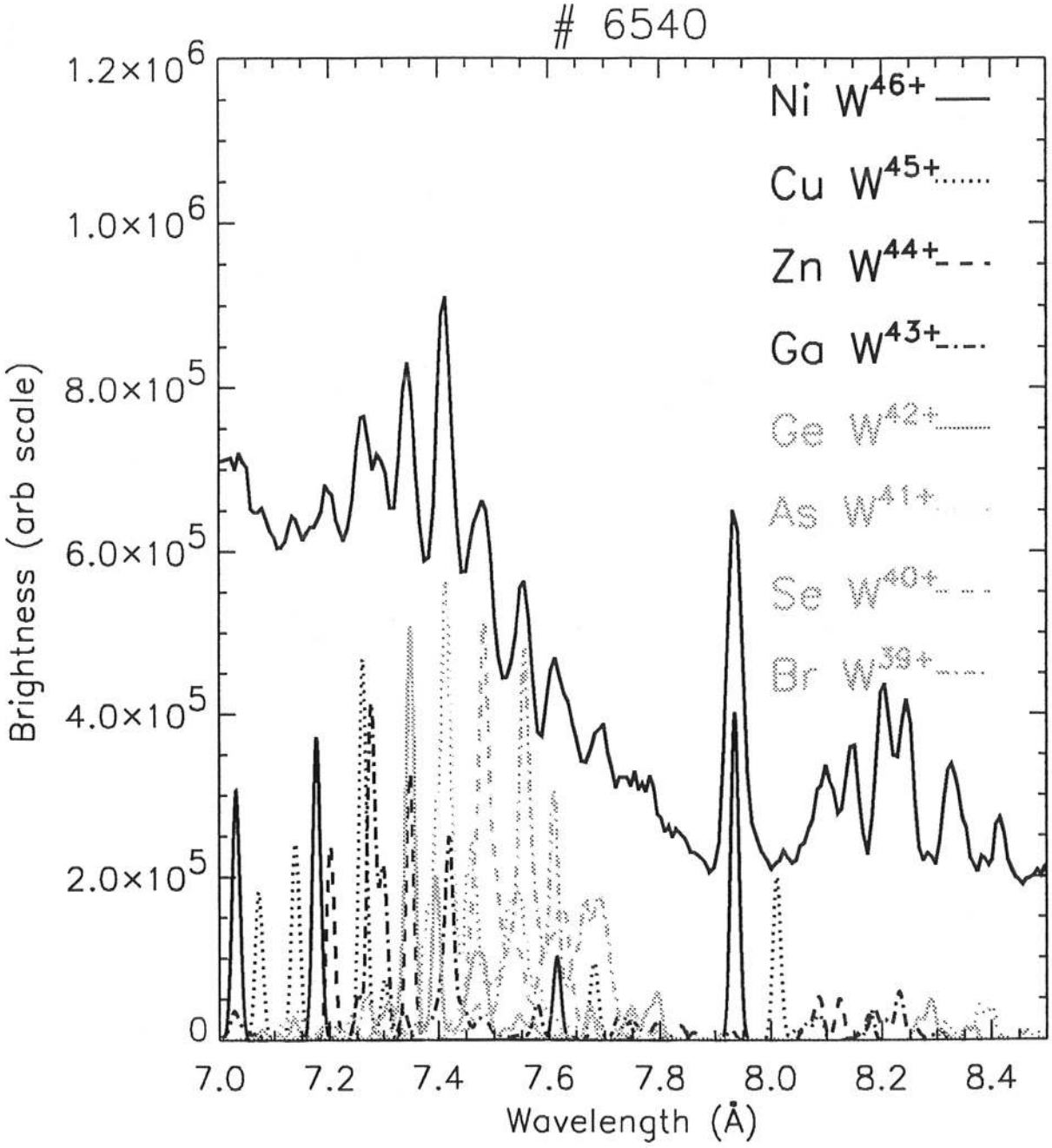

Figure 3: a) X-ray spectra of tungsten together with the theoretical predictions, in the range from 7.0 to 8.5 Å measured with a KAP crystal (discharge #6540).

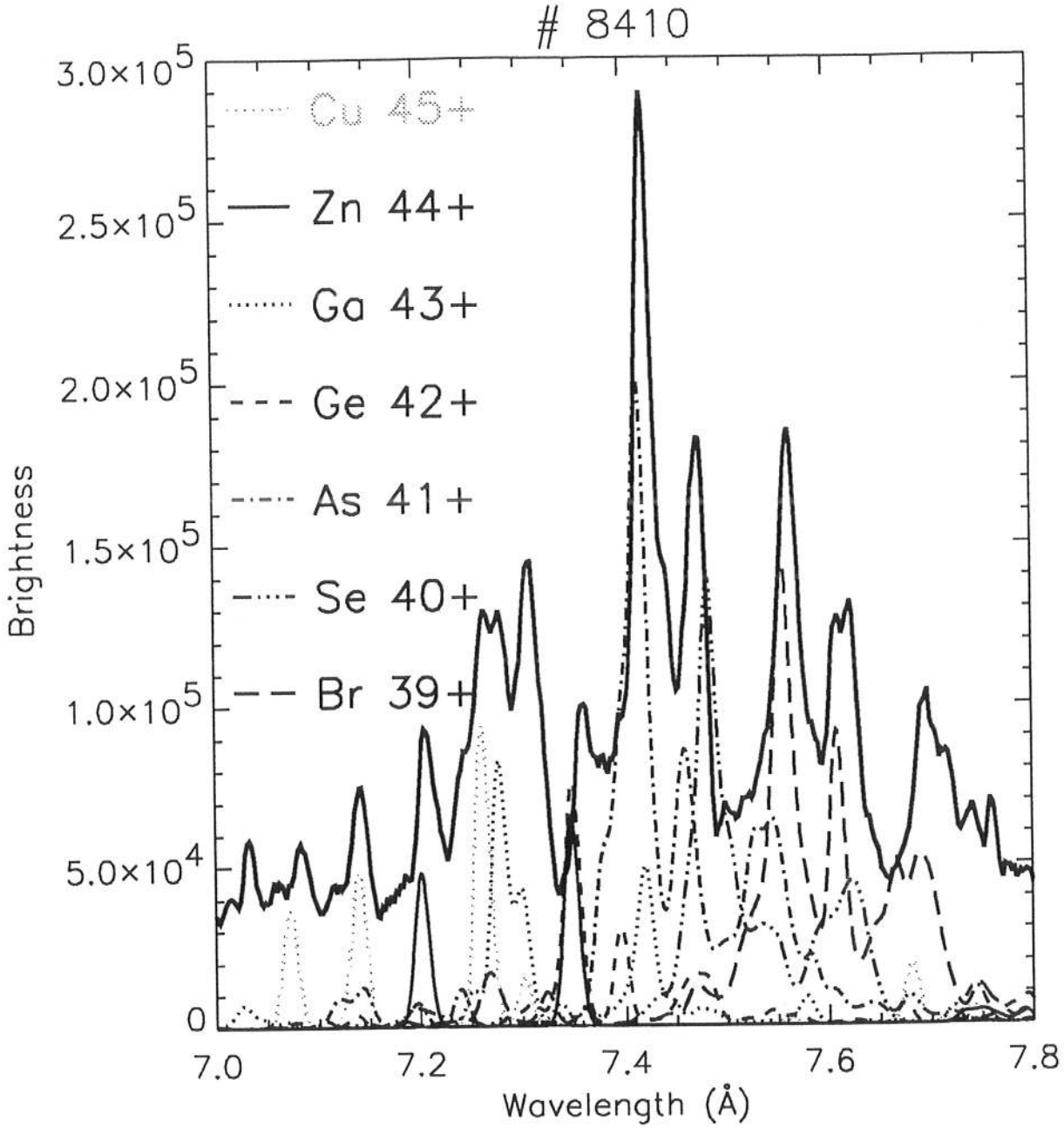

Figure 3: b) X-ray spectra of tungsten together with the theoretical predictions, in the range from 7.0 to 7.8 Å measured with a ADP crystal (discharge #8410).